Wholly biobased polyamide thermoplastic elastomer-cellulose nanocomposites

Nurhamiyah, Y., Yoon, S., & Chen, B. (2022). Wholly biobased polyamide thermoplastic elastomer-cellulose nanocomposites. *Macromolecular Materials and Engineering*, Article 2200120. https://doi.org/10.1002/mame.202200120

Published in:
Macromolecular Materials and Engineering

Document Version:
Peer reviewed version

WILEY-VCH

Wholly Biobased Polyamide Thermoplastic Elastomer-Cellulose Nanocomposites

*Yeyen Nurhamiyah, Sungkwon Yoon and Biqiong Chen**

Dr Y. Nurhamiyah, Dr S. Yoon, Prof. B. Chen
School of Mechanical and Aerospace Engineering, Queen's University Belfast, Stranmillis Road, Belfast, United Kingdom
*Email: b.chen@qub.ac.uk

Dr Y. Nurhamiyah
Research Center for Biomass and Bioproducts, National Research and Innovation Agency, Jl. Raya Bogor Km. 46 Cibinong, Bogor, Indonesia

Keywords: nanocomposite, elastomer, cellulose, polyamide, biobased polymer

Abstract

Polymers play a prominent role in our daily lives, however there is a growing concern on the depleting fossil resources triggering the effort to search for their sustainable substitutions. Here, we prepared novel wholly biobased nanocomposites from polyamide 36,36 (PA36,36) thermoplastic elastomer and cellulose nanocrystals (CNCs). The influence of CNC addition and CNC loading on the morphological features, thermal and mechanical properties of PA36,36 was studied. The presence of CNC in PA36,36 affected the thermal degradation of PA36,36. The additions of 10 wt.% and 30 wt.% CNCs to the PA36,36 improved the tensile strength and Young's modulus by up to 700% and 750% to 9.6 MPa and 6.8 MPa, respectively, while still maintaining relatively high elongation at break values. The hardness of the polymer increased significantly after the inclusion of CNC. The PA36,36/CNC nanocomposites also showed relatively good resilience when exposed to 100% strain. Overall, these biobased thermoplastic elastomer nanocomposites could be potential alternatives for some existing rubbers with low or medium hardness.

1. Introduction

Since their discovery in the 20th century, polymers have been continuously used in our daily lives as they offer lightweight, high-performance, and cost-effective materials. Polymers are nearly used in every field such as clothing, buildings, transportation, packaging, communication, food, energy, health and many more. The polymer production reached 368 million tonnes in 2019, and this number hugely escalates compared to the production in 1960, which was only 15 million tonnes.[1,2] However, this significant production number comes along with consequences such as air and water pollution from the petrochemical industry, and the rapidly depleting fossil resources as energy demand continues to increase.[3] Thus, sustainable resources and production methods are strongly needed to help eliminate these concerns.

There are a number of renewable resources that are currently under exploration including the raw materials of biobased polymers such as lignocellulose, starch, plant oil, chitosan, and biomass waste.[4] Recently, we synthesised a novel sustainable thermoplastic elastomer, namely polyamide 36,36 (PA36,36) from biobased fatty diamine (Priamine 1075) and biobased fatty acid (Pripol 1009).[5] PA36,36 shows remarkable properties such as large elongation at break (up to 2286%), high toughness and good hydrophobicity, and displays autonomous self-healing behavior at ambient temperature. While promising for applications such as stretchable conductors, flexible sensors, coating and elastic textiles, this material is considered too soft (Shore A and Shore D hardness = 16 and 6, tensile strength = 1.27 MPa) for applications which require higher hardness and higher strength. Thus, it is necessary to improve the hardness and tensile strength of PA36,36 to broaden its potential applications.

Cellulose nanocrystals (CNCs) are derived from plant cellulose fibres, cellulose microcrystals (MCC), and wood fibres, through acid hydrolysis.[6] They have excellent properties such as low density, high tensile strength (7.5 – 7.7 GPa),[6] high elastic modulus (~150 GPa),[7] large surface area, ubiquity and high reactivity.[6,8] As a renewable material with outstanding

properties, CNC is a promising filler to reinforce the biobased PA36,36 while maintaining the material's sustainability.

In this work, PA36,36/CNC nanocomposites were prepared through solution casting with different CNC concentrations. The addition of CNCs into the biobased polyamide matrice is expected to increase the strength and hardness and extend the applications of the polymer. The wholly biobased nanocomposites were characterised with Scanning Electron Microscopy (SEM), Fourier Transform Infrared (FTIR) spectroscopy, Differential Scanning Calorimetry (DSC), Thermogravimetric Analysis (TGA), quasi-static tensile testing, cyclic tensile testing, and Shore A and D hardness tests.

2. Results and Discussion

2.1 *Cellulose nanocrystals*

The morphology and the geometric dimensions of CNCs prepared from sulfuric acid hydrolysis of MCCs were studied by SEM (**Figure 1a**). CNC is a rodlike material with length of 50 – 500 nm and width of 3 – 5 nm. The average length and diameter of the CNCs are estimated to be 286.1 ± 34.1 nm and 22.2 ± 2.9 nm, respectively. Therefore, the average aspect ratio of the CNCs is 12.9, consistent with previous reports.[6,9-11] The average length and diameter of the CNCs are much smaller than those for MCCs (the inset of Figure 1a), which are 47.7 ± 8.5 μm and 17.6 ± 5.8 μm, respectively. These results initially imply that the acid hydrolysis process has successfully converted MCC into CNC.

The chemical structure of the CNCs and MCCs was characterized by FTIR, and their spectra are presented in **Figure 1b**. CNC displays the characteristic absorption bands of cellulose reported in the literature.[12-14] For example, the absorption peak of CNC at 3353 cm^{-1} is assigned to O-H stretching and at 1062 cm^{-1} related to C-O-C asymmetric stretching.[13] The absorption peaks of CNC are similar to those of MCC, except for a small peak at 810 cm^{-1}

which is assigned for S-O due to the effect of sulphuric acid hydrolysis.[15] This result further confirms the successful preparation of CNC from MCC.

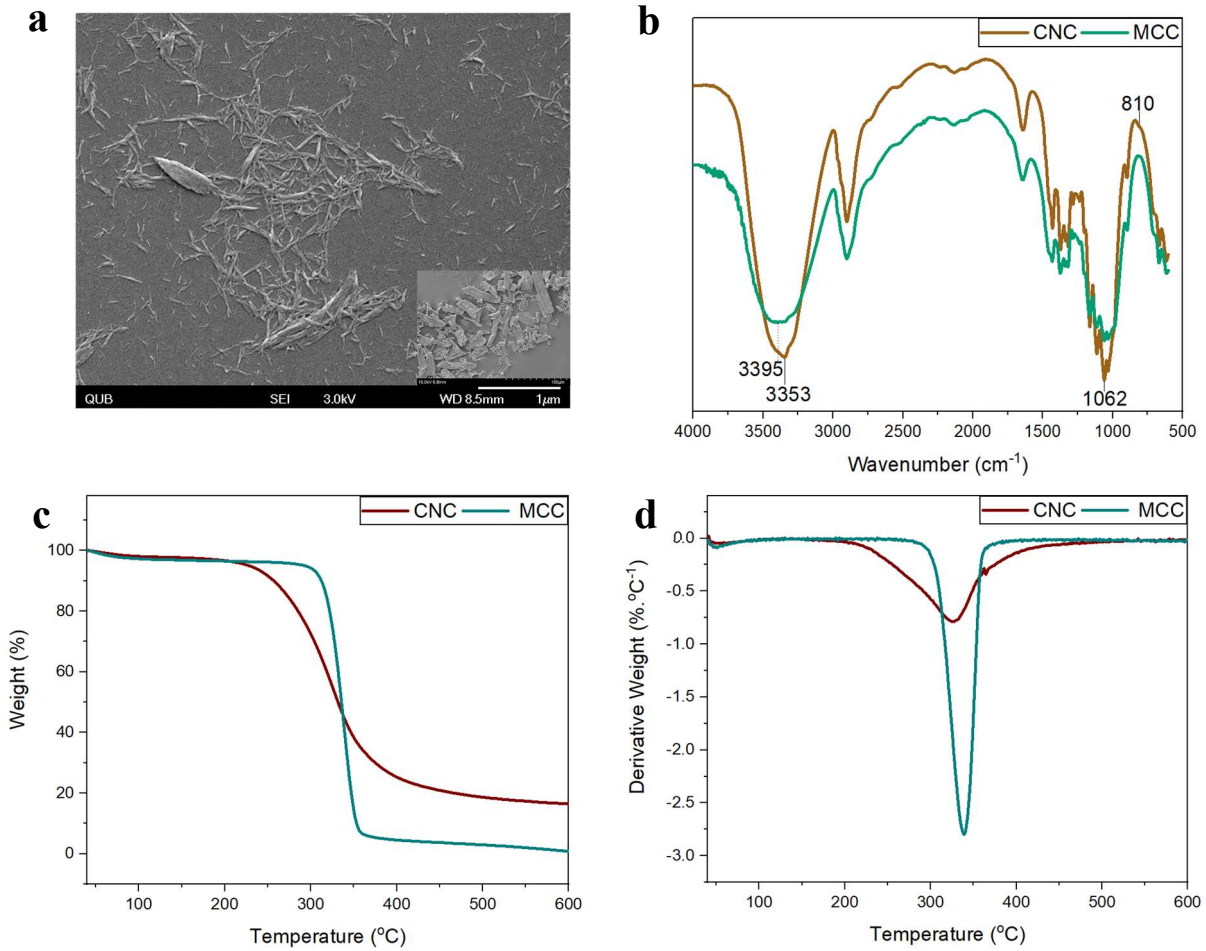

Figure 1. Characterization of CNC and MCC: (a) SEM images (inset: MCC), (b) FTIR spectra, (c) TGA thermograms, and (d) DTG curves.

The TGA and derivative thermogravimetry (DTG) results of CNCs are presented in **Figure 1c**, **1d**. CNC begins the mass loss at 120 ºC due to evaporation of water. The acid hydrolysis shows a significant effect on the thermal degradation behavior of CNC. The onset degradation temperature (T_d^{onset}) of CNC is observed at 255 ºC, which is lower than that of MCC (310 ºC). The peak degradation temperature (T_d^{peak}) of CNC is 327 ºC, 12 ºC lower than the value for MCC. Sulphuric acid is used in acid hydrolysis because the negative sulphate groups create a stable suspension of CNCs and break down the cellulose into rodlike nanoparticles.[16,17] However, sulphate groups are also responsible for reduction of the thermal stability of cellulose, as the elimination of sulphuric acid in sulphated anhydroglucose occurs at a much lower

temperature.[18] The amount of char residue at 600 °C in CNC is 16.7% which is higher than that of MCC (0.8%). This high amount of char residue could act as the flame insulator and leads to CNC with better flame retardancy than MCC.[16]

2.2 PA36,36/CNC nanocomposites

Surface morphology

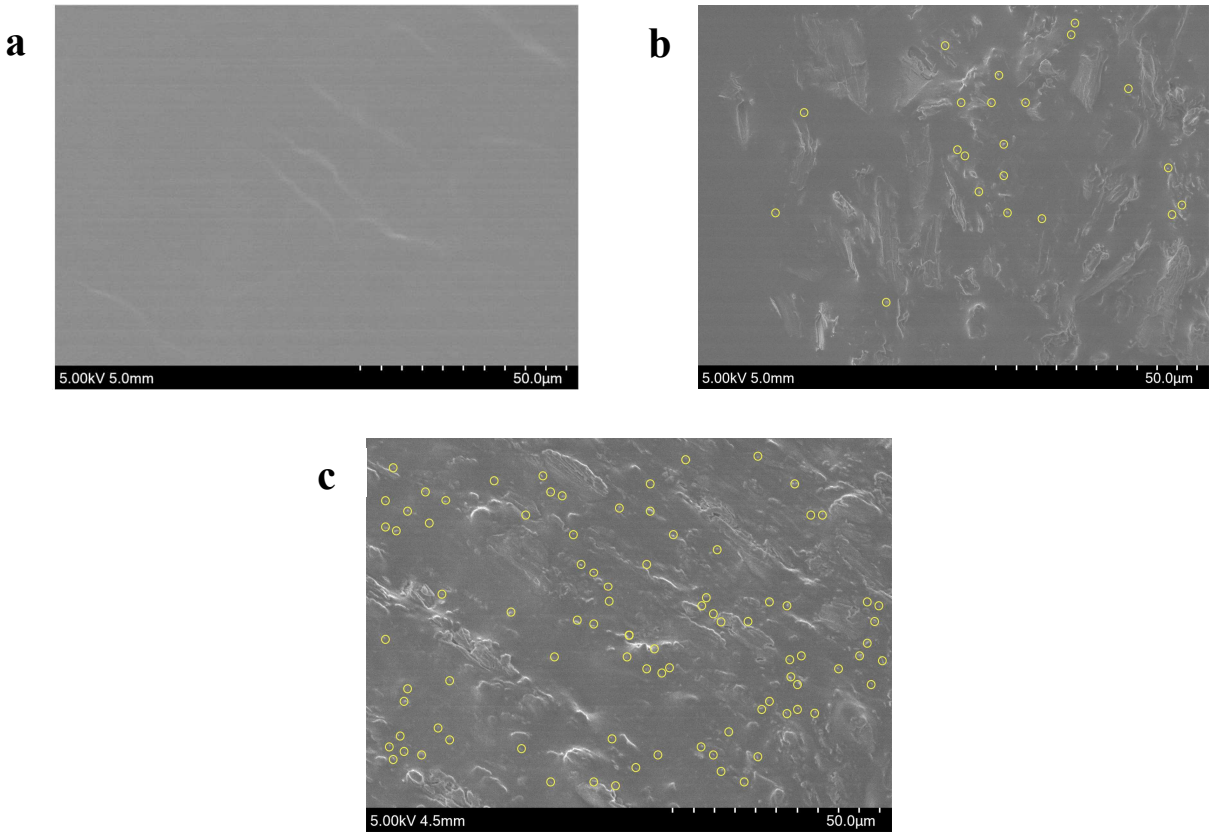

Figure 2. SEM images of the cryo-fractured surface of: (a) PA36,36, and PA36,36/CNC nanocomposites with CNC contents of (b) 10 wt.% and (c) 30 wt.%. The yellow circles indicate CNCs within the samples.

To evaluate the CNC dispersion in PA36,36, the morphology of the cryo-fractured surface of PA36,36 and PA36,36/CNC nanocomposites was observed by SEM (**Figure 2**). Under the same magnification, neat PA36,36 displays a fractured surface with fewer features when compared to the two nanocomposite samples. For the two nanocomposite samples, CNCs (within yellow circles) are detected as well dispersed small rod-like particles in the micrographs. With the content of CNC increasing from 10 wt.% to 30 wt.%, more CNC particles are observed.

Chemical structure

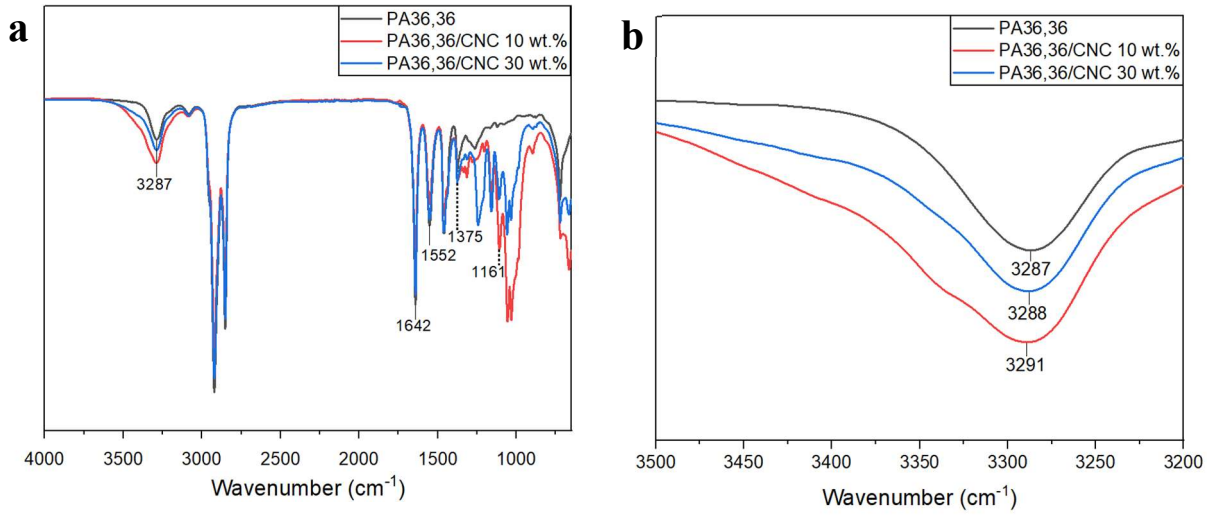

Figure 3. FTIR spectra of PA36,36 and PA36,36/CNC nanocomposites in the range of (a) 4000-650 cm^{-1} and (b) 3500-3200 cm^{-1}.

The FTIR spectra of the neat PA36,36 and PA36,36/CNC nanocomposite are presented in **Figure 3**. Based on our previous work,[5] the characteristic absorption bands of polyamide at 3287 cm^{-1}, 1642 cm^{-1}, 1552 cm^{-1}, 1425 cm^{-1} and 1281 cm^{-1} are attributed to N-H stretching from amide A, C=O stretching from amide I, N-H bending of amide II, and N-H bending from amide III, respectively. The evidence of CNC in the nanocomposites is given by the peak at 1375 cm^{-1} assigned to the vibration of C-O aromatic ring, and the absorptions between 1000 cm^{-1} and 1250 cm^{-1} attributed to C–O–C (ether) assymetric stretching.[19,20]

The existence of these characteristic peaks of CNC in the spectra of PA36,36/CNC nanocomposites proves the successful integration of CNC into PA36,36. The peak at 3287 cm^{-1} for N-H stretching in PA36,36 shifts to a higher wavenumber at 3291 cm^{-1} in PA36,36/CNC nanocomposites, implying the strong interaction between PA36,36 and CNC because of hydrogen bonding between the N-H from the former and O-H from the latter.[19] **Figure 4** illustrates the hydrogen bonding between the PA36,36 and CNC.

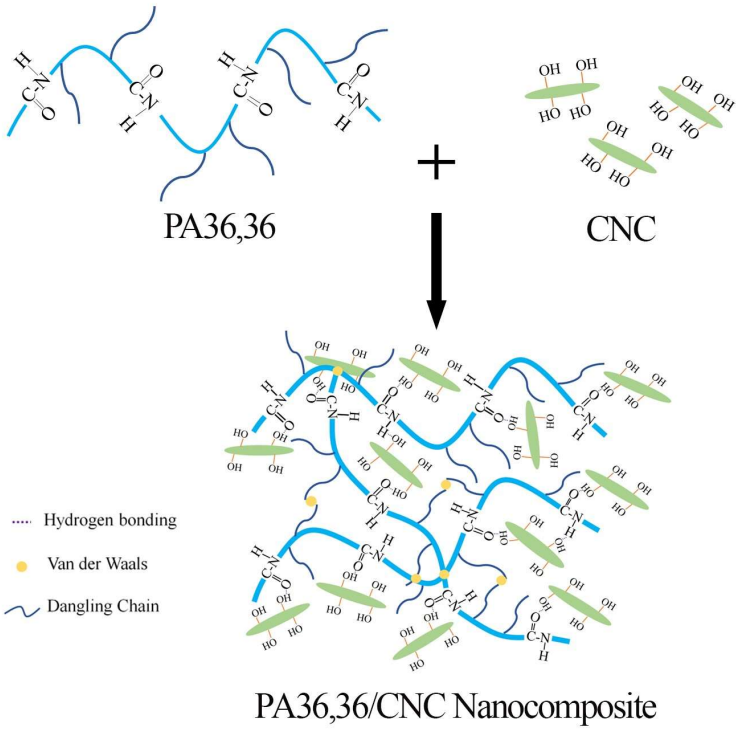

Figure 4. Schematic illustration of the interfacial interaction by hydrogen bonding between PA36,36 and CNC in the nanocomposites and the formation of a physical network due to hydrogen bonds and multiple van der Waals bonds.

Thermal properties

To investigate the thermal properties, PA36,36 and its CNC nanocomposites were analyzed by both DSC and TGA. The second heating curves from DSC are presented in **Figure 5a**. No melting or crystallization transition was observed in the samples, indicating an amorphous polymer, in line with our previous report.[5] Each repeating unit of PA36,36 consists of a long methylene chain and four dangling chains, which make this polymer branched and amorphous.[5] The T_g of PA36,36, determined from the onset of the glass transition, is −25.8 °C, lower than the value determined from dynamic mechanical analysis on the polymer without solution processing.[5] The addition of CNC to the polymer slightly lowers its T_g, to −26.4 °C and −26.9 °C for the nanocomposites with CNC contents of 10 wt.% and 30 wt.%, respectively.

Reduction of T_g by the addition of CNC has previously been reported for poly(acrylic acid), which was attributed to increased segment mobility.[21]

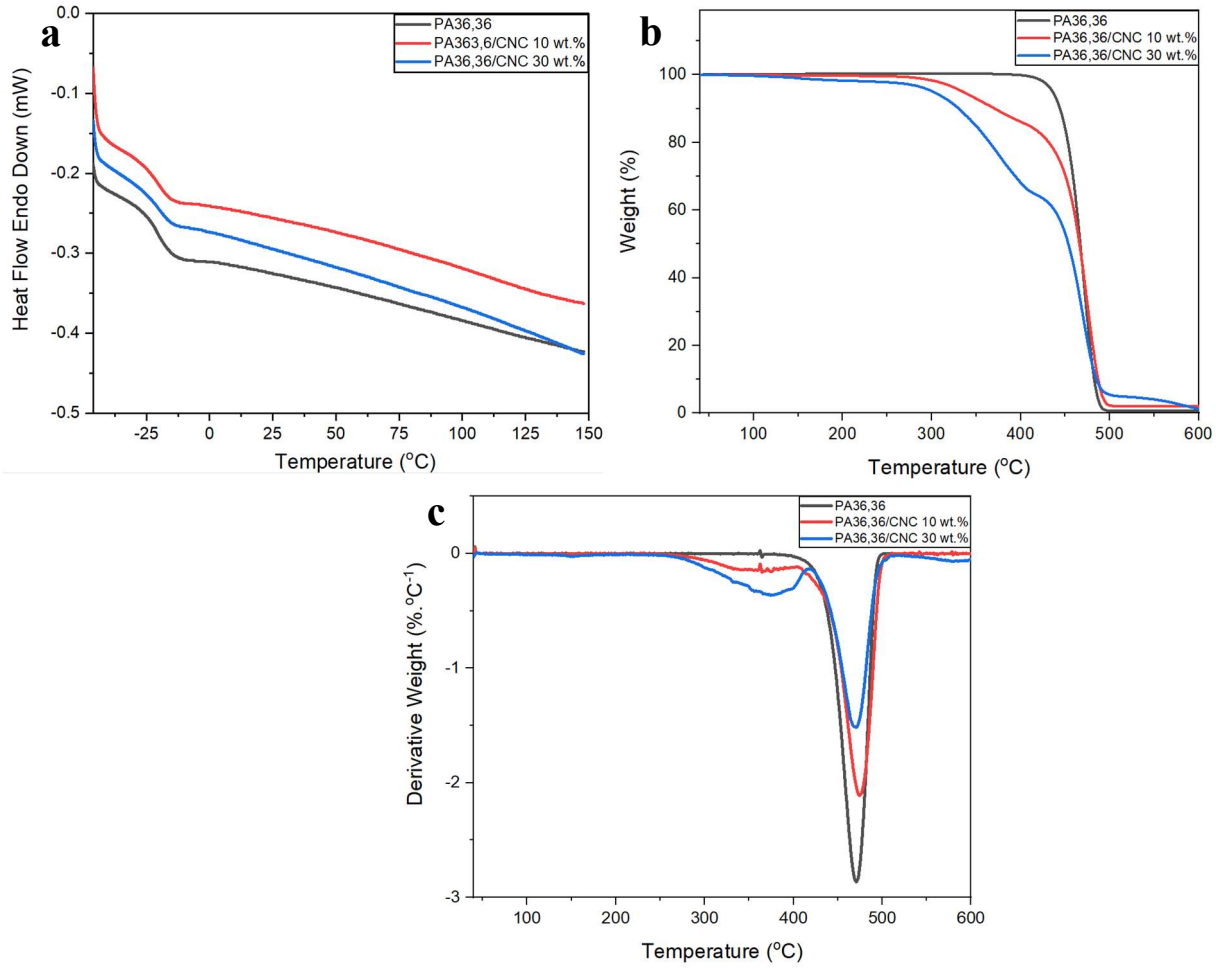

Figure 5. Thermal analysis of PA36,36 and PA36,36/CNC nanocomposites with different CNC contents: (a) DSC second heating, (b) TGA and (c) DTG thermograms.

The influence of CNC on the thermal stability of PA36,36 was investigated by TGA which is depicted in **Figure 5b**. The PA36,36 shows a single thermal degradation with T_d^{onset} at 438 °C.[5] The nanocomposites show two-step degradations with the first onset degradation occurring at 312 °C and 309 °C for the CNC contents of 10 wt.% and 30 wt.%, respectively, which is related to the degradation of CNC. The second onset degradation is observed at 445 °C and 447 °C for filler contents of 10 wt.% and 30 wt.% which is linked to the degradation of PA36,36.

From the DTG thermograms (**Figure 5c**), it is observed that compared to the neat polymer the nanocomposites have an additional decomposition peak of CNC at 365 °C for PA36,36/CNC 10 wt.% and 374 °C for PA36,36/CNC 30 wt.%, which are higher than T_d^{peak} of CNC. For the second degradation peak of the nanocomposites, the addition of CNC increased T_d^{peak} of PA36,36 from 471 °C[5] to 475 °C in PA36,36/CNC 10 wt.%, which could be attributed to the strong bonding between the polymer and CNC.[22] In contrast, T_d^{peak} of PA36,36/CNC 30 wt.% remained similar (470 °C) to that of PA36,36 due to the oppositing effects of the strong interfacial bonding and the lower thermal stability of CNC.

Tensile properties

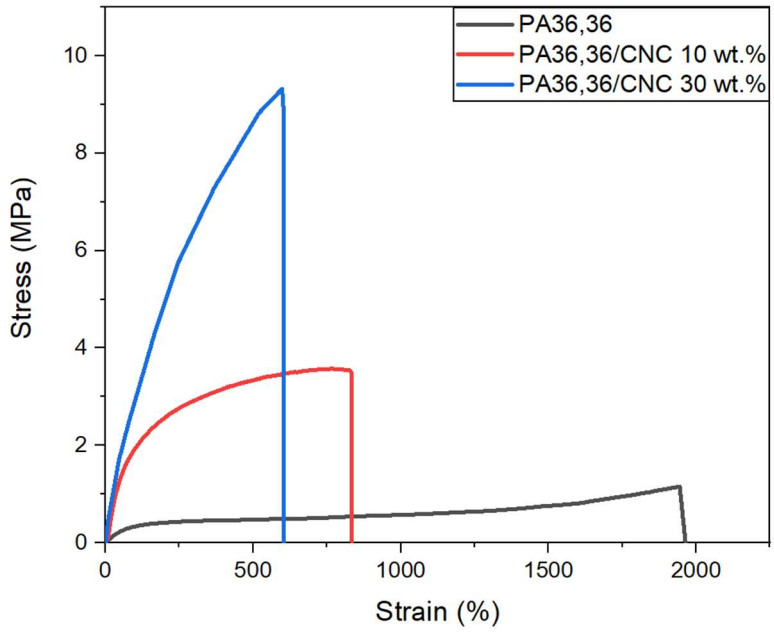

Figure 6. Representative tensile curves of PA36,36 and PA36,36/CNC nanocomposites.

The tensile profiles of the neat PA36,36 and its nanocomposite samples were studied at ambient temperature (**Figure 6**). In contrast to neat PA36,36, the nanocomposites exhibit noticeable improvements in tensile strength and Young's modulus, with lower ductility. The tensile strength of the neat PA36,36 is 1.2 ± 0.1 MPa, while for PA36,36/CNC 10 wt.% and PA36,36/CNC 30 wt.% are 3.4 ± 0.1 MPa and 9.6 ± 0.2 MPa, respectively (**Table 1**). The enhancement in tensile strength is associated with the effective load transfer from PA36,36 to

CNC due to strong interfacial interaction by hydrogen bonding between amide groups of the polymer and hydroxyl groups of CNC as discussed earlier (**Figure 4**).

Young's modulus of PA36,36/CNC nanocomposites increased significantly along with the CNC content. The Young's modulus increases from 0.8 ± 0.2 MPa for the neat polymer, to 3.4 ± 0.2 MPa for PA36,36/CNC 10 wt.% and 6.8 ± 0.8 MPa for PA36,36/CNC 30 wt.%, indicating stiffening effect of CNC in nanocomposites.[23] These improvements are associated with the high modulus (~150 GPa)[7] and aspect ratio (12.9) of CNC and a good dispersion of CNC in polymer matrix. The difference in the Young's modulus of the neat polymer from the value reported before[5] is due to the solution processing method used in this work, which might have caused disentanglement and rearrangement of some polymer chains, reducing the physical crosslinks in the polymer.[24]

The elongation at break of PA36,36/CNC decreases significantly with the increasing content of CNC, meaning that the nanocomposites become less ductile compared to neat PA36,36. The elongation at break decreases from 1915% for the polymer to 829% for 10 wt.% CNC content and 586% for 30 wt.% CNC content. During tensile deformation, CNC gives confinement effect that restricts chain flexibility.[25] However, these elongation at break values are still considered relatively high.

Table 1. Mechanical properties of PA36,36 and PA36,36/CNC nanocomposites.

Sample Name	Tensile strength (MPa)	Young's Modulus (MPa)	Elongation at Break (%)	Energy at Break ($MJ.m^{-3}$)	Hardness (Shore A/Shore D)
PA36,36	1.2 ± 0.1	0.8 ± 0.2	1915 ± 150	11.9 ± 0.6	16/6
PA36,36/CNC 10 wt.%	3.4 ± 0.1	3.4 ± 0.2	829 ± 64	23.2 ± 1.7	30/10
PA36,36/CNC 30 wt.%	9.6 ± 0.2	6.8 ± 0.8	586 ± 20	35.7 ± 1.6	65/30

The nanocomposites possess similar tensile stress-strain curves to some existing rubbers such as ethylene propylene diene monomer (EPDM) rubber,[26] and styrene butadiene rubber

(SBR).[27] The tensile strength of PA36,36/CNC 10 wt.% is higher than the values for EPDM and polydimethyl siloxane (PDMS) which are 2.4 MPa,[26] and 1.1 MPa,[28] respectively. Meanwhile PA36,36/CNC 30 wt.% has higher tensile strength than a silicone rubber (4.9 MPa)[29] and nitrile butadiene rubber (NBR) (7.7 MPa)[30] but is comparable to higher hardness rubber such as (SBR) (10 MPa).[31] The elongation at break values of PA36,36/CNC 10 wt.% and PA36,36/CNC 30 wt.% are higher than EPDM (388%),[26] PDMS (128%)[28], silicone rubber (500%),[29] NBR (~370%),[30] and SBR (184%).[31] The results (summarized in **Figure 7**) show that with higher tensile strength than EPDM and PDMS, PA36,36/CNC 10 wt.% still maintained remarkable stretchability, while PA36,36/CNC 30 wt.% showed higher stretchability and strength in comparison to NBR and SBR. PA36,36/CNC nanocomposites could be used for the applications which require comparable tensile strength with the above-mentioned rubbers but higher stretchability such as stretchable electronics and soft robots.[32] Compared to the neat PA36,36 with energy at break of 11.9 $MJ.m^{-3}$, the addition of CNC increases energy at break by up to 200% to 35.7 $MJ.m^{-3}$. This result is higher than a silicone rubber with a fracture energy of 19.6 $MJ.m^{-3}$.[33]

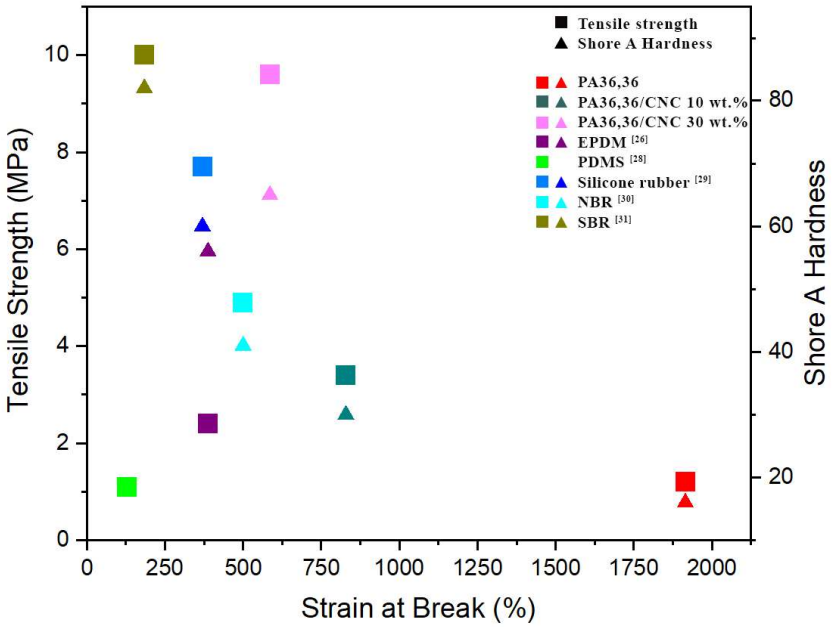

Figure 7. The comparison of tensile strength and Shore A Hardness versus the strain at break of PA36,36 and its cellulose nanocomposites with several commercial rubbers.

Unlike neat PA36,36, the nanocomposites did not display self-healing ability at ambient temperature after two broken pieces had been brought in contact for a period of 24 h. This is because the presence of the high contents of CNCs could act as barriers and hinder the diffusion of polymer chains across the fracture surfaces.[34,35] This limits the formation of abundant van der Waals bonds between chains which are responsible for the self-healing behavior of neat PA36,36.[5] Introducing heat to the broken pieces when in contact may facilitate the healing process of the nanocomposites.

Hardness

The reinforcing effect of CNC on PA36,36 is also observed in the enhancement of hardness (**Table**). The addition of CNC to PA36,36 matrix increases the hardness significantly. Loading 10 wt.% CNC to PA36,36 increases Shore A hardness by around 90% of its original values from 16 to 30, and loading 30 wt.% increases Shore A hardness by 310% to 65. Meanwhile, the addition of 10 wt.% CNC increases the Shore D hardness by 60% from 6 to 10, and addition of 30 wt.% increases Shore D hardnness by 400% to 30. The improvement in hardness of the nanocomposites is related to the stiffening effect of the CNC which is also spotted in the increasing trend in Young's modulus.[23] Compared to the rubber materials mentioned earlier, the nanocomposite with 10 wt.% CNC loading has a lower Shore A hardness. The Shore A hardness for silicone rubber, NBR and EPDM are 41,[28] ~62,[29] and 56.[26] However, PA36,36/CNC 30 wt.% nanocomposite has higher or comparable Shore A hardness with these rubbers (**Figure 7**).

Resilience

In order to study the resilience of PA36,36/CNC nanocomposites, cyclic tensile tests were performed up to a strain level of 100% and the results are illustrated in **Figure 8**. **Figure 8a** shows the testing result of PA36,36/CNC 10 wt.% nanocomposite with five repeated loading-unloading cycles. The nanocomposites follow a typical nonlinear stress-strain behavior under the first loading-unloading cycle where the stress softening takes place. The following cycles

experience further stress reduction and almost stabilise from the fourth cycle. Meanwhile the cyclic testing result of PA36,36/CNC 30 wt.% (**Figure 8b**) displays a slightly non-linear stress-strain curve with stress softening in the first cycle. This kind of curve is also spotted in EPDM rubber.[35] The stress reduction in the second cycle is not as much as that in PA36,36/CNC 10 wt.% and from the third cycle the stress almost stabilizes. These results suggest these nanocomposites have relatively good resilience and shape recovery after two or three cycles.

As described before, PA36,36 consists of long entangled main chains and multiple dangling chains. Such a "supramolecular" structure creates plenty van der Waals bonds and few hydrogen bonds, leading to the formation of dynamic physical crosslinks and so a thermoplastic elastomer.[5] The presence of CNCs introduces more hydrogen bonds to the physical crosslinks (**Figure 4**), maintaining the elastomeric behavior and a relatively good shape recovery in the polymer nanocomposites.

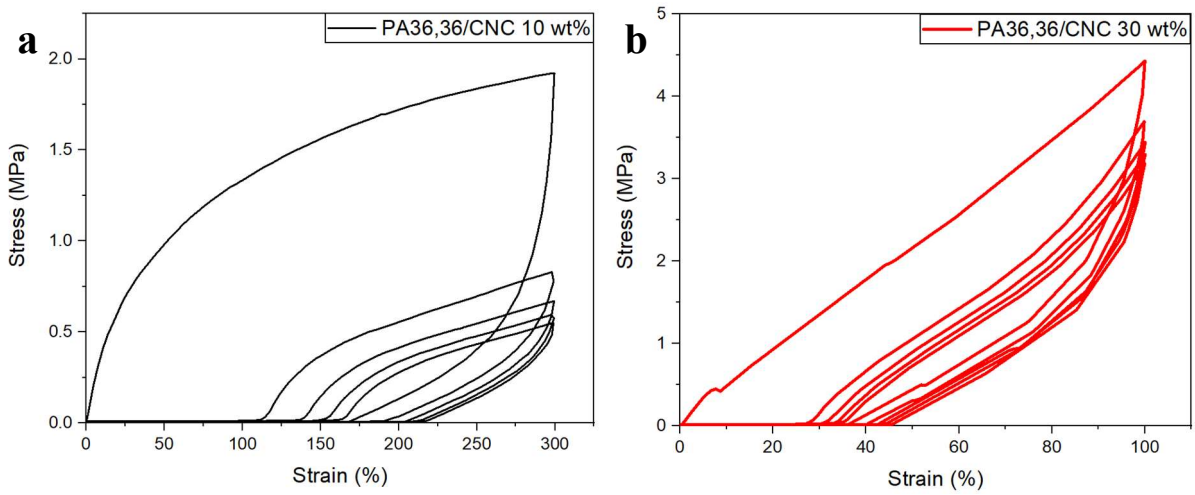

Figure 8. Stress-strain curves from cyclic tensile tests up to a strain of 100% for PA36,36/CNC nanocomposites: (a) 10 wt.%, and (b) 30 wt.%.

Large hysteresis loop is observed in both nanocomposites in the first cycle, implying a significant energy dissipation due to the rupture of hydrogen bonding of CNC networks during tensile deformation.[37-39] The rearrangement of the dissociated networks takes time to recover its original state,[37] leaving a residual strain. The hysteresis loop for cycle two onward was

much smaller. The area between the loading and unloading curves was employed to measure the energy dissipation during the tensile deformation. The energies dissipated in the first cycle of PA36,36/CNC 10 wt.% and PA36,36/CNC 30 wt.% are 0.51 $MJ.m^{-3}$ and 1.36 $MJ.m^{-3}$, respectively, which are reduced significantly for subsequent cycles. This result is similar to the finding reported in a previous study, where the increasing of CNC content in a poly(acrylic acid) resulted in a rise of energy dissipation in the first cycle.[40] The CNCs acted as temporary physical crosslinks which upon tensile deformation were largely dissociated increasing the energy dissipation.[37,41] A higher energy dissipation is beneficial for these elastomer nanocomposites to be used in shock absorption applications.[42]

The hysteresis ratio (h_r) is calculated by the ratio of the energy dissipation (e_d) to the energy absorption (i.e. the area below the loading curve, e_a), *i.e.*, equation (1)[43].

$$h_r = \frac{e_d}{e_a} \tag{1}$$

For the nanocomposite with 10 wt.% CNC, h_r is reduced from 0.82 for the first cycle to 0.70 − 0.63 in the subsequent cycles, while for the PA36,36/CNC 30 wt.% h_r decreases from 0.63 in the first cycle to 0.44 − 0.38 in the subsequent cycles. A higher loading of CNC shows a lower hysteresis ratio, implying better resilience.[44] These biobased nanocomposites with relatively good resilience may also find applications where wear resistance and shape recovery are important.[45] Pre-stretching of the samples could be conducted to reduce the initial hysteresis ratios as it induces the rupture of the weaker bonds between the polymer and CNC[46] and helps orient CNCs towards the stretching direction. Furthermore, allowing a relaxation for a certain duration (*e.g.*, 10 − 30 min) after each cycle may help recover the original shape of the nanocomposite samples.[5]

In addition, PA36,36/CNC nanocomposites show excellent hydrophobicity depsite their high CNC contents. After being immersed in water for 24 h the samples showed no water absorption . This is in agreement with the superior hydrophobicity and coating behavior of PA36,36 we

previously reported,[5] as well as the strong bonding between PA36,36 and CNC that facilitates excellent coating of the hydrophobic polymer onto the hydrophilic CNC.

3. Conclusions

Biobased polyamide/cellulose nanocomposites were prepared by solution casting of PA36,36 with CNC contents of 10 wt.% and 30 wt.%. CNC was obtained through the acid hydrolysis of cellulose microcrystalline with sulphuric acid, which was confirmed by FTIR and SEM.

The CNC filler reduced the T_g of the polymer slightly, and introduced an additional small thermal degradation step at a lower temperature; however, it maintained or increased the peak thermal degradation temperature for the main polymer degradation step. The tensile strength of PA36,36 was significantly improved by up to 7 times to 9.6 MPa due to effective stress transfer from the polymer matrix to CNC filler. The additions of CNC also provided an enhancement of Young's modulus by up to 7.5 times to 6.8 MPa because of the high modulus of CNC. While decreased from the value for the neat polymer, the elongation at break of the nanocomposites still maintained at relatively high elongation at break, being 829% for 10 wt.% CNC and 586% for 30 wt.% CNC. Shore A hardness of the nanocomposites increased significantly from 16 to 65 with 30 wt.% CNC loading, and Shore D hardness increased from 6 to 30 for the same nanocomposite. Both PA36,36/CNC nanocomposites also showed good resilience and shape recovery after two or three cycles up to 100% strain, and a higher CNC content increased the energy dissipitation but reduced hysteresis ratio.

The enhancement of the mechanical properties in the PA36,36/CNC nanocomposites is significant, which make them attractive renewable and recyclable alternatives to some existing fossil-based elastomers and chemically crosslinked rubbers with low or medium hardness.

4. Experimental Section

4.1 *Materials*

MCC with particle size of 20 μm and tetrahydrofuran (THF, Emplura) were supplied by VWR UK. Sulphuric acid (98%, H_2SO_4) and potassium bromide (KBr) (FTIR grade, ≥99% trace metals basis) were provided by Sigma-Aldrich. The polymer used as the matrix (PA36,36(24 h)) was prepared and characterized as described in our earlier publication.[5] The PA36,36 has a weight average molecular weight of 142,400 $g.mol^{-1}$, and a number average molecular weight of 40,300 $g.mol^{-1}$.[5]

4.2 *Methods*

Preparation of cellulose nanocrystals

CNC was prepared by sulphuric acid hydrolysis using methods reported in the literature.[47-49] Briefly, MCC (5 g) was mixed with 100 g of 64 wt.% H_2SO_4 at 45 ºC for 1 h using a magnetic hot plate stirrer. The mixture was diluted with 500 ml of distilled water and the CNC was collected after centrifugation at 6000 rpm for 20 min (Hermle Z 206 A). CNC was then washed with distilled water several times by centrifugation until reaching neutral pH. The resulting CNC paste was stored for further use. To calculate the CNC content in the paste, a small amount of CNC paste was weighed and dried in a convection oven for 24 h at 60 ºC.

Preparation of PA36,36/CNC nanocomposites

Polyamide nanocomposites were prepared following a published method.[50] The CNC paste was washed with THF three times using a centrifuge at 6000 rpm for 20 min. A desired amount of washed CNC was placed in a beaker and dispersed in THF (10 ml) using a sonication bath (Fisherbrand) for 60 min, making a CNC/THF suspension. Separately, PA36,36 was dissolved in THF (100 ml) in a beaker covered with parafilm and stirred with a magnetic stirrer for 24 h at ambient temperature. The CNC/THF suspension was mixed into the PA36,36/THF solution which was stirred for 20 h at ambient temperature with the beaker covered and another 4 h with the beaker open to let the solvent gradually evaporate. Then, the remaining solution was poured

into a Teflon Petri dish and left in a fume cupboard to evaporate and obtain nanocomposite films.

4.3 *Characterization*

SEM of the CNC sample was performed on a JEOL JSM 6500F at an accelerating volatge of 3 kV. SEM of the MCC, PA36,36 and nanocomposites was carried out on a Hitachi FLEX SEM 1000 at 5 − 15 kV. The CNC and MCC samples were each dispersed in distilled water at a concentration of 0.01 w/v % and a droplet of the suspension was placed on an aluminum stub which was left to evaporate in a fume cupboard, followed by gold coating using an Agar Auto Sputter Coater. The PA36,36 and nanocomposite specimens were cryo-fractured under a liquid nitrogen cooling condition. A conductive carbon tape and a conductive silver paste (Ted Pella, USA) were used to mount the specimens on aluminum stubs.

The functional group characterization of CNC and MCC was conducted on a Perkin Elmer Spectrum 100 FTIR. Each of MCC and CNC powder was mixed with KBr which was then pressed into a disc. FTIR was performed in transmission mode and scan range of 4000 – 650 cm^{-1}. All samples were recorded with 64 scans with a resolution of 4 cm^{-1}. The spectra of the polymer and the nanocomposites were recorded using the same equipment but with attenuated reflectance mode.

TGA was conducted on a Q50 TGA instrument (TA Instruments) under the flow of nitrogen at a rate of 50 $ml.min^{-1}$. The weight loss of the samples (16 − 32.0 mg) was recorded by heating the samples up to 600 °C at a heating rate of 10 $°C.min^{-1}$. DSC was performed on a DSC 25 (TA Instruments), with 5 − 10 mg of samples. All samples received two heating-cooling cycles between −50 °C and 150 °C, with a heating or cooling rate of 10 $°C.min^{-1}$, under a nitrogen flow at a rate of 50 $ml.min^{-1}$. The second heating cycle was used for analysis.

The tensile testing of the nanocomposites was performed on a Lloyds LRX universal testing machine equipped with a 500 N load cell. The tests were carried out at ambient temperature (16

°C) with a crosshead speed of 100 mm.min^{-1}. Square sheets of PA36,36/CNC nanocomposite with dimensions 10 cm x 10 cm x 0.5 mm were prepared using a Rondol heated hydraulic press. A desired amount of PA36,36/CNC nanocomposites were placed in a mould between the hydraulic press platens, heated to 120 °C and pressed for 4 min. Subsequently, the sheets were cut into dumb-bell shape according to ISO-37 type 3, by using a punching machine. At least three specimens were tested for each material. Cyclic tensile testing was performed on the same equipment at ambient temperature with a testing speed of 10 mm.min^{-1}. The test was conducted up to 100% strain for five cycles on each sample. Shore A and Shore D hardness tests were carried out on a Coats Comaco Rubber Harness tester in accordance with ISO-868. The tests were repeated three times.

Acknowledgements

YN thanks the Indonesia Endowment Fund for Education (LPDP) for a PhD scholarship.

Received: ((will be filled in by the editorial staff))
Revised: ((will be filled in by the editorial staff))
Published online: ((will be filled in by the editorial staff))

References

[1] Plastics Europe. Plastic - the Facts 2020. (2020).

[2] M. Hong, E. Y.-X Chen, *Green Chem*. **2017**, 19, 3692.

[3] C. Okkerse, H. Van Bekkum, *Green Chem*. **1999**, 1, 107.

[4] R. Mülhaupt*, Macromol. Chem. Phys*. **2013,** 214, 159.

[5] Y. Nurhamiyah, A. Amir, M. Finnegan, E. Themistou, M. Edirisinghe, B. Chen, *ACS Appl. Mater. Interfaces*. **2021**,13, 6720.

[6] R. J. Moon, A. Martini, J. Nairn, J. Simonsen, J. Youngblood, *Chem. Soc. Rev*. **2011**, 40, 3941.

[7] S. Iwamoto, W. Kai, A.Isogai, T. Iwata, *Biomacromolecules* **2009**, 10, 2571.

[8] H. Liu, D. Liu, F. Yao, Q. Wu, *Bioresour. Technol*. **2010**, 101, 5685.

[9] Z. Man, N. Muhammad, A. Sarwono, M. A. Bustam, M. V. Kumar, S. Rafiq, *J. Polym. Environ*. **2011**, 19, 726.

[10] L. Du , J. Wang,Y. Zhang , C. Qi , M. P. Wolcott, Z. Yu, *Nanomaterials* **2017**, 7, 51.

[11] S. Shrestha, F. Montes, G. T. Schueneman, J. F. Snyder, J. P. Youngblood, *Compos. Sci. Technol*. **2018**, 167, 482.

[12] P. Lu, Y.-L. Hsieh, *Carbohydr. Polym*. **2010**, 82, 329.

[13] A. Kumar, Y. S. Negi, V. Choudhary, N. K. Bhardwaj, J. Mater. Phys. Chem. **2014** 2, 1.

[14] Z. Mo, Z. Zhao, H. Chen, G. Niu, H. Shi, *Carbohydr. Polym.* **2009**, 75, 660.

[15] D. Gaspar, S. N. Fernandes, A. G. de Oliveira, J.G Fernandes, P. Grey, R. V. Pontes, L. Pereira, R. Martins, M. H. Godinho, E. Fortunato, Nanotechnology **2014**, 25, 94008.

[16] M. Roman, W. T. Winter, *Biomacromolecules* **2004**, 5, 1671.

[17] N. Wang, E. Ding, R. Cheng, *Polymer* **2007**, 48, 3486.

[18] M. R. K Sofla, R.J Brown, T. Tsuzuki, T. J. Rainey, *Adv. Nat. Sci. Nanosci. Nanotechnol*. **2016,** 7, 035004.

[19] T. Wu, M. Frydrych, K. O'Kelly, B. Chen, *Biomacromolecules* **2014**, 15, 2663.

[20] C. J. Grande, F. G.Torres, C. M. Gomez, O. P. Troncoso, J. Canet-Ferrer, J. Martínez-Pastor, *Mater. Sci. Eng. C* **2009**, 29 1098.

[21] S. Soman, A.S. Chacko, V.S. Prasad, *Compos. Sci. Technol.* **2017***,* 14, 65.

[22] A. Kaushik, D. Ahuja, V. Salwani, *Compos. Part A Appl. Sci. Manuf*. **2011**, 42, 153.

[23] N. Gray, Y.Hamzeh, A. Kaboorani, A. Abdulkhani. *Ind. Crops Prod*. **2018**, 115, 298.

[24] C. Birck, S. Degoutin, N. Tabary, V. Miri, M.Bacquet*, Express Polym. Lett.* **2014**, 8, 12, 943.

[25] P. Rittigstein, R. D.Priestley, L.J. Broadbelt, J.M. Torkelson, *Nat. Mater.* **2007**, 6, 278.

[26] P. Li, L. Yin, G. Song, J. Sun, H. Wang, *Appl. Clay Sci*. **2008**, 40, 38.

[27] J. Krajči, , Z. Špitálský, and I. Chodák, *Eur. Polym. J.* **2014**, *55*, 135.

[28] S. Wu, S. Peng, C. H. Wang, *Sensors Actuators A Phys.* **2018**, 279, 90.

[29] M. Frounchi, S. Dadbin, F. Panahinia, *Nucl. Instruments Methods Phys. Res. Sect. B Beam Interact. with Mater. Atoms* **2006,** 243, 354.

[30] X. Cao, C. Xu, Y. Wang, Y. Liu, Y. Liu, Y. Chen, *Polym. Test.* **2013**,32, 819.

[31] A. Zanchet, L.N. Carli, M. Giovanela, J. S. Crespo, C. H. Scuracchio, R. C. R. Nunes, *J. Elastomers Plast*. **2009**, 41, 497.

[32] Z. Wang, C. Xiang, X. Yao, P. Le Floch, J. Mendez, Z. Suo, *Proc. Natl. Acad. Sci.* **2019**, 116, 5967.

[33] S. Ziraki, S. M. Zebarjad, M. J. Hadianfard, *J. Mech. Behav. Biomed. Mater.* **2016**, 57, 289.

[34] T. Wu, B. Chen, *RSC Adv*. **2017**, 7, 20422.

[35] T. Wu, B. Chen, *ACS Appl. Mater. Interfaces* **2016**, 8, 24071.

[36] M. Cheng, W. Chen, Int. *J. Solids Struct*. **2003**, 40, 4749.

[37] J. Yang, C.-R.Han, J.-F. Duan, F. Xu, R.-C. Sun, *ACS Appl. Mater. Interfaces* **2013**, 5, 3199.

[38] J. Yang, C. Shao, L. Meng, *Langmuir* **2019**, 35, 10542.

[39] J. Murai, T. Najima, T. Matsuda, K. Tsunodae, T. Nonoyama, T. Kurokawa, J. P. Gong , *Polymer* **2019**, 178, 121686.

[40] J. Yang C. R. Han J. F. Duan, M. G. Ma, X. M. Zhang, F. Xu, R. C Sun, X. M. Xie, *J. Mater. Chem*. **2012**, 22, 22467.

[41] J. Yang, C.-R. Han, X.-M. Zhang, F. Xu, R.-C. Sun, *Macromolecules* **2014**, 47, 4077

[42] X. Zhou, L. Wang, X. Cao, Q. Yin, G. Weng, *J. Appl. Polym. Sci.* **2019**, 136, 47278

[43] Y. Nurhamiyah, G. Irvine, E. Themistou, B. Chen, *Macromol. Chem. Phys*. **2021**, 222, 2100218.

[44] J. Moon, S. B. Kwak, J. Y. Lee, D. Kim, J. U. Ha, J. S. Oh, *Waste Manage.* **2019,** *85*, 557.

[45] S. Rios, R. Chicurel, L.F. Del Castillo, *Mater. Des.* **2001**, 22, 369.

[46] J. Diani, B. Fayolle, P. Gilormini, *Eur. Polym. J.* **2009**, 45, 601.

[47] S. Beck-Candanedo, M. Roman, D. G. Gray, *Biomacromolecules* **2005**, 6, 1048.

[48] M. A. S. Azizi Samir, F. Alloin, J.Y. Sanchez, N. El Kissi, A. Dufresne, A. *Macromolecules* **2004**, 37, 1386.

[49] D. Bondeson, A. Mathew, K. Oksman, *Cellulose* **2006**,13, 171.

[50] T. Wu, Y. Su, B. Chen, *ChemPhysChem* **2014**, 15, 2794.